INSTITUTE OF PHYSICS PUBLISHING PHYSICS IN MEDICINE AND BIOLOGY

Phys. Med. Biol. **50** (2005) 441–458 doi:10.1088/0031-9155/50/3/004

Voxel model in BNCT treatment planning: performance analysis and improvements

Sara J González[1], **Daniel G Carando**[2], **Gustavo A Santa Cruz**[1] **and Robert G Zamenhof**[3]

[1] UAIC, Centro Atómico Ezeiza, Comisión Nacional de Energía Atómica, Av. Del Libertador 8250, (1429) Ciudad de Buenos Aires, Argentina
[2] Departamento de Matemática, Universidad de San Andrés, Vito Dumas 284, (1644) Victoria, Buenos Aires, Argentina
[3] Department of Radiation Oncology, Tufts-New England Medical Center, 750 Washington Street, Box 246, Boston, MA 02111, USA

E-mail: srgonzal@cnea.gov.ar and daniel@udesa.edu.ar

Received 18 October 2004, in final form 2 December 2004
Published 12 January 2005
Online at stacks.iop.org/PMB/50/441

Abstract

In recent years, many efforts have been made to study the performance of treatment planning systems in deriving an accurate dosimetry of the complex radiation fields involved in boron neutron capture therapy (BNCT). The computational model of the patient's anatomy is one of the main factors involved in this subject. This work presents a detailed analysis of the performance of the 1 cm based voxel reconstruction approach. First, a new and improved material assignment algorithm implemented in NCTPlan treatment planning system for BNCT is described. Based on previous works, the performances of the 1 cm based voxel methods used in the MacNCTPlan and NCTPlan treatment planning systems are compared by standard simulation tests. In addition, the NCTPlan voxel model is benchmarked against in-phantom physical dosimetry of the RA-6 reactor of Argentina. This investigation shows the 1 cm resolution to be accurate enough for all reported tests, even in the extreme cases such as a parallelepiped phantom irradiated through one of its sharp edges. This accuracy can be degraded at very shallow depths in which, to improve the estimates, the anatomy images need to be positioned in a suitable way. Rules for this positioning are presented. The skin is considered one of the organs at risk in all BNCT treatments and, in the particular case of cutaneous melanoma of extremities, limits the delivered dose to the patient. Therefore, the performance of the voxel technique is deeply analysed in these shallow regions. A theoretical analysis is carried out to assess the distortion caused by homogenization and material percentage rounding processes. Then, a new strategy for the treatment of surface voxels is proposed and tested using two different irradiation problems. For a parallelepiped phantom perpendicularly irradiated with a 5 keV neutron source, the large

thermal neutron fluence deviation present at shallow depths (from 54% at 0 mm depth to 5% at 4 mm depth) is reduced to 2% on average. Reassigning fluence values in the case of this phantom in angular position produced the maximum deviation in the thermal fluence to decrease from 140% to 23% at the surface of the phantom. Thus, even for the largest deviations, obtained by intentionally placing the phantom in the most disadvantageous position with respect to the voxel grid, the reassignment shows very good performance. Since these results substantially improve the performance of the 1 cm based voxel model in surface boundary regions, the proposed strategy will be implemented in future versions of the NCTPlan code.

1. Introduction

Boron neutron capture therapy (BNCT) is a form of radiotherapy that poses a unique challenge for optimizing the treatment of each individual patient (Locher 1936, Wazer *et al* 1994, Zamenhof *et al* 1999). Since the radiation dose field combines high- and low-LET radiation acting on different length scales, detailed dosimetry calculations are significantly more complicated than in conventional external beam radiotherapy.

The mathematical description of the transport of neutrons through matter comprises the solution of the integrodifferential form of the transport equation. Although this equation provides the exact description of the particle density in the phase space, it is virtually impossible to find an explicit solution even for relatively simple geometries. The complexity of the problem usually demands the use of numerical techniques such as the discrete-ordinates method or statistical simulation (Monte Carlo) methods (Duderstadt and Martin 1979).

Among the discretization techniques used historically in neutron transport modelling, mesh representations and homogenization methods provided satisfactory solutions, but with an unavoidable loss of fine-scale information (Moulton 1996, Moran *et al* 1992). Nevertheless, the degree of accuracy achieved can be improved if physical and geometrical information is appropriately managed in the generation of the model. Such is the goal of this work.

Treatment planning systems (TPS) based on Monte Carlo methods appeared as the principal candidate tool in BNCT (Zamenhof *et al* 1996, Kiger *et al* 1996, Nigg *et al* 1999). Monte Carlo calculations allow the complex radiation transport problem to be treated accurately, tracking millions of particles and computing each dose component. Currently, there are several developments of planning codes either based on Monte Carlo or deterministic methods (Kumada *et al* 2004, Cerullo and Daquino 2001, van der Zee *et al* 2002, Kotiluoto *et al* 2001, Ingersoll *et al* 1997). Some of these systems have been used clinically, and many of these latter systems use the so-called voxel reconstruction method to simulate the real geometry (Mackerle 2003, Smith 1986). As a common method employed in different TPS for BNCT, it was the subject of study in various published related works, in which the influence of the voxel size and material mixing was assessed using standard simulation tests as reference data (Goorley *et al* 2001b, 2002, Wojnecki and Green 2002). In short, these works showed that the voxel method is accurate enough for deriving the dosimetry when a voxel size of 1 cm^3 or smaller is used, and clinical-like geometries are analysed. However, Wojnecki and Green (2002) also reported that the spatial resolution used by the voxel reconstruction technique implemented in MacNCTPlan TPS (Kiger III *et al* 1996), which is 1 cm^3, may lead to differences of up to 20% in the thermal neutron fluence for a rectangular phantom irradiated through one of its sharp edges.

The question of how good the accuracy of the voxel method is to derive the patients' dosimetry is not limited to the question of how much the voxel size and material mixing affects the particle transport itself. In order to assess the dosimetry for every point in the geometry, there are other factors that need to be taken into account. Basically, the whole process comprises the creation of the voxel model from a set of CT images, the calculation of average particle fluence or dose in every cell, and finally a method that extrapolates estimates to any point inside the geometry model. The voxel model involves the selection of the voxel size and the strategy used to assign a homogeneous material to each cell. The calculation of particle fluence and doses involves the selection of the Monte Carlo engine (typically MCNP code (Briesmeister 1997)), the tally volume (e.g., the volume of material cells), the assignment of the average values to a point inside the tally volume (typically, the centre of the volume) and the assumption that absorbed doses can be approximated by kerma (ICRU 1999).

In view of the aspects just mentioned, this work presents a detailed analysis of the performance of the voxel reconstruction method for a fixed voxel size of 1 cm^3, with a special emphasis on the effect of the material homogenization on surface boundary areas. First, an improved algorithm for the voxelization process is introduced, which is implemented in NCTPlan TPS (González *et al* 2002) (the new version of MacNCTPlan code). Then, it is shown that the MacNCTPlan material assignment algorithm is mainly responsible for the thermal fluence 20% deviation reported in Wojnecki and Green (2002), rather than the spatial resolution of 1 cm^3 itself. Indeed, it is demonstrated that the degree of accuracy of the 1 cm based voxel method, with a more suitable material assignment algorithm, is much better than 20% in a range of depths wider than the one studied in Wojnecki and Green (2002). Moreover, the accuracy of the voxel approach can be improved by choosing an appropriate position of the voxel grid with respect to the analysed geometry. Therefore, since the voxel method with the new material assignment algorithm is the strategy used by NCTPlan TPS, rules to get the best performance in treatment planning are also discussed. In addition, a comparison of an in-phantom experimental dosimetry performed at the RA-6 reactor of Argentina and the corresponding dosimetry simulations is performed. Besides being a realistic situation in terms of geometry and particle source description, this allows us to benchmark the voxel model against reference data obtained by means other than computational methods.

The surface boundary areas are those where homogenization can have a more distorting effect (this fact was also remarked in Kumada *et al* (2004)). One of the main reasons is that air is the most different material from the point of view of particle transport. Taking this into account, a theoretical analysis is carried out to assess the distortion caused by homogenization and also to estimate the errors due to rounding the proportions of each material. A new strategy is proposed to substantially improve the performance of the voxel model in surface regions.

2. Materials and methods

2.1. Geometry modelling technique: material assignment model

The voxelization technique used by MacNCTPlan to create the Monte Carlo model from CT medical images has been described in detail in Zamenhof *et al* (1996) and Kiger *et al* (1996). Since the main difference between the MacNCTPlan and NCTPlan voxel methods is the material mixing assignment, the following focuses on the material homogenization process.

The original strategy followed by the MacNCTPlan voxel reconstruction algorithm can be summarized as follows. For each voxel, the algorithm computes the real proportions of the four primary material types in it (i.e., air, bone, tumour and normal tissue) from CT images, and rounds each proportion to a 20% volume increment. If the rounded percentages sum to

100%, they are assigned to the current voxel. If not, the algorithm assigns the previous voxel's material mixture to the current cell. Clearly, this approach can lead to serious errors in the material model.

The strategy followed by the NCTPlan voxel reconstruction algorithm is based on the search for an '*admissible mixture*' that minimizes the following expression:

$$\sum_{i=1}^{4} \left| \frac{X_i^{\text{real}} - X_i^{\text{rounded}}}{X_i^{\text{real}}} \right| \tag{1}$$

where X_i^{real} and X_i^{rounded} are the real and rounded proportions of primary material type i, respectively. This expression represents the sum of the absolute values of the relative material percentage differences.

When the set of X_i^{rounded} are the nearest rounded percentages, expression (1) is minimized, and the algorithm tries this configuration as its first choice. If this configuration is not an admissible mixture assignment (i.e., the rounded percentages do not sum to 100%), the algorithm adjusts the rounded percentages subject to the following criteria: (a) the original rounded percentage for air (i.e., the nearest rounded value) will not be changed since it is desirable to leave unchanged the material considered most dissimilar in terms of affecting particle transport and (b) if the real proportion of a material is zero, this material will not be created since it would be unnatural to introduce a material into a cell where it is not actually present.

The strategy followed is to evaluate which material percentage is more convenient to adjust in terms of reaction rates, i.e., to keep the macroscopic cross section as close as possible to the real case. Among all the nuclides composing the four basic material types, hydrogen (H) and nitrogen (N) are the two most important for neutron transport. While nitrogen mainly contributes to neutron capture reactions (^{14}N(n, p)^{14}C), hydrogen contributes to both neutron capture and scattering reactions (^{1}H(n, γ)^{2}H, ^{1}H(n, n$'$)^{1}H). In addition, since ^{10}B is explicitly included in the Monte Carlo model because of its high neutron capture cross section, it is also considered in the strategy.

Considering only neutron capture reactions in H and N, the ratios of adult brain to adult skeleton-cranium or adult muscle to adult femur macroscopic cross sections are greater than 1 for ICRU 46 material compositions (ICRU 1992). That means the number of reactions per unit time and volume in soft tissue is greater than that in bone (by $\sim$10%), and thus the algorithm should adjust the bone percentage. The same applies for boron capture and neutron scattering reactions since boron and hydrogen contents in soft tissue are greater than those in bone. Therefore, taking into account all the reactions of interest in this analysis, it will be advantageous to adjust bone percentage and maintain the soft tissue original rounded proportion.

The previous analysis was done for the case in which the algorithm must decide to adjust percentages of soft tissue and bone. Applying the same reasoning as above, if tumour and normal tissue are compared, the algorithm adjusts the percentage of the latter since both tissues have the same elemental composition but a different boron concentration (a 3.5 tumour-to-normal ^{10}B ratio is typically used in clinical treatments (Coderre and Morris 1999)).

To summarize the final algorithm's strategy for inadmissible mixtures, bone percentage is adjusted over soft tissue, and normal tissue is adjusted over tumour.

2.2. Numerical test problems

Wojnecki and Green (2002) have studied the performance of the MacNCTPlan voxel model for a parallelepiped phantom irradiated with monoenergetic and monodirectional neutron beams

of 50 mm radius. This performance was assessed comparing thermal neutron fluences along the beam axis against the data derived for the exact geometry modelled by the reference computational tool MCNP. In order to evaluate the performance of the proposed algorithm and compare it with the older version, it was subjected to the same tests.

A water-filled rectangular phantom of 140 × 150 × 190 mm^3 and 8 mm polymethylmethacrylate walls was used in the simulations. Two different positions of the parallelepiped phantom with respect to the particle source were evaluated (referred to as 'parallel' and 'angular' positions). In the first case, particles are perpendicularly directed onto one face of the phantom while in the angular case, particles bombard one of its edges. Note that in the case of the angular position, the CT images of the phantom are rotated with respect to the parallel position leading to two different material models of the same geometry. All simulations were carried out for a 5 keV monodirectional beam of 50 mm radius, and 10 million histories were sampled in each run. Thermal neutron fluence profiles along the beam axis were used as the figure of merit for the comparisons. In the case of voxel models, the tally volume coincides with the volume of the homogenized cells, which is 1 cm^3. On the other hand, reference data were computed for two different tally volumes, in a cylinder of 2 mm diameter and 1 mm high (in the following referred to as 'punctual' fluence), and in a cubic cell of 1 cm edge (referred to as 'averaged' fluence).

As mentioned above, the material model that results from a CT study depends on the position of the voxel grid with respect to the position of the images. Then, the thermal fluence along the beam axis could be affected for this reason. For the completeness of the evaluation, different positions of the voxel grid were analysed. In the case of the parallel position, simulations were carried out for 10 locations of the voxel grid, starting with a voxel edge coincident with the phantom's entrance face (position 0), and moving the edge each 1 mm (positions 1–9). Following the same procedure, 10 locations of the voxel grid were also computed in the case of the angular position.

2.3. Dosimetry comparisons against experimental data

With the aim of providing a more complete idea of the accuracy of the voxel model in a clinical-like case, results of a comparison between the in-phantom experimental dosimetry performed at the RA-6 BNCT facility in Argentina (Blaumann *et al* 2004) and the corresponding computational dosimetry calculations are presented.

To obtain dose-rate values in every cell of the voxel representation, average flux tallies are usually modified by energy-dependent response functions which convert the average flux in a cell to average dose rate. These response functions, for neutrons and photons, are the fluence-to-kerma coefficients that account for the initial kinetic energy for all those primary charged particles released by uncharged particles (ICRU 1999).

Dose calculations in the voxel model and experimental measurements involved in this comparison are performed with the assumption that charged particle equilibrium (CPE) conditions (Attix 1986) are satisfied everywhere in the geometry. Under this assumption, dose is approximated by kerma. This condition is readily fulfilled for neutrons of low to moderate energies such as those present in a typical BNCT beam but not for photons, especially in interfaces (i.e., build-up regions), where the actual dose delivered is lower than the corresponding kerma value. With the assumption of CPE, the photon dose in the first few millimetres of tissue close to the interface with air will be overestimated by the calculations, which in a sense constitutes a conservative position in terms of normal tissue dose tolerance. A rough estimation of this difference for the RA-6 beam indicates that the total maximum equivalent dose to normal tissue at 5 mm depth is overestimated at most 2.4% by the kerma value.

The Argentine BNCT facility is currently dedicated to the treatment of cutaneous melanoma (González *et al* 2004), and has been designed in order to provide a *hyperthermal* flux with a maximum thermal flux at shallow depths (Blaumann *et al* 2004). As part of its characterization, detailed experimental dosimetry was performed by neutron flux and dose measurements in a water-filled acrylic cylinder phantom, using foil activation and paired ionization chamber techniques (Attix 1986, Rogus *et al* 1994). The results of the physical dosimetry, given by thermal neutron flux, fast neutron and total gamma absorbed dose rate profiles along the central beam axis, were used as the experimental reference data in this work. The comparisons for the dose-rate components are made for those points inside the model where CPE conditions are fulfilled for photons. In the case of thermal neutron flux measurements, an additional point on the surface of the phantom was included. The computational model has been generated from a set of CT images of the cylindrical phantom, employing water and acrylic compositions (Attix 1986). The computational radiation source described by discretized distributions was used to compute profiles along the beam axis (Blaumann *et al* 2004). Both gamma and fast neutron absorbed dose rates were specified for ICRU 46 adult muscle tissue (ICRU 1992).

2.4. Theoretical analysis on surface boundary regions

One natural consequence of the voxelization and homogenization procedures is the directional bias due to the cubic distortions introduced by partitioning a 3D geometry. For example, the 1 cm^3 voxel model of a filled sphere transforms its original smooth surface to a more stepwise surface. In addition, the volume and surface area of the voxelized sphere are always larger than those of the real ones, since most voxels lying in surface regions that share the interior and exterior of the sphere are assigned a homogenized material other than air. These kinds of distortions and expansion effects mainly affect surface boundary areas. Therefore, it is reasonable to expect the voxel method to degrade in accuracy near boundary regions where fine-scale information would be desirable.

The aim of this section is to propose a different strategy to better adjust the average fluence in the surface cells and therefore, to improve the prediction of the punctual fluence within the first millimetres of the surface. A theoretical analysis of a parallelepiped phantom is carried out, taking into account the effects of homogenization and percentage rounding in the voxel model. This analysis will suggest the strategy to follow.

2.4.1. Material homogenization. As a first approach to the problem, consider an infinite p cm thick slab ($0 < p < 1$) of material M and macroscopic total cross section Σ^M, perpendicularly irradiated with an infinite planar neutron or photon source (figure 1(a)). Now consider the voxel model of the slab that results from positioning the voxel grid in such a way that all the slab is contained in a layer l of voxels (figure 1(b)). Before rounding the percentages of material M and air, each of the cells in l contains a proportion p of M and $(1 - p)$ of air. The first step in the analysis is to determine how the average fluence for a slab portion of 1 cm^2 cross section and p cm thick is compared with the average fluence in a 1 cm^3 voxel of the homogenized slab.

To assess the effect of homogenization only, eventual rounding is ignored for the moment. The result of the voxelization is a new slab, which is 1 cm thick and is made of a homogeneous material M^* (figure 1(c)). The macroscopic total cross section of this mixture is $\Sigma^{M^*} = (1 - p)\Sigma^{\text{air}} + p\Sigma^M$, where Σ^{air} is the macroscopic total cross section of air. Since $\Sigma^{\text{air}} \ll \Sigma^M$, the value of Σ^{M^*} is well approximated by $p\Sigma^M$. Now, the mean free path of a particle in the homogenized slab is $\lambda^* = 1/\Sigma^{M^*} \approx 1/(p\Sigma^M) = \lambda/p$, where λ is the mean

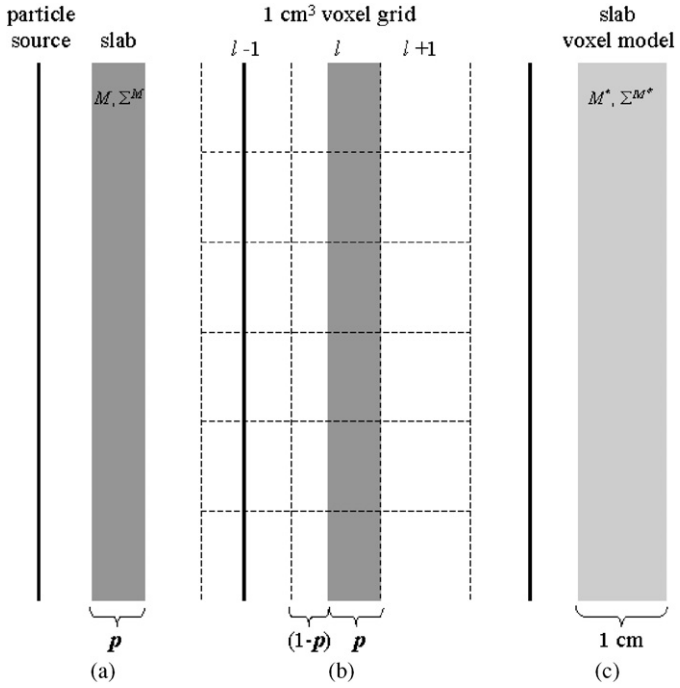

Figure 1. (a) Infinite p cm thick slab ($0 < p < 1$) perpendicularly irradiated with an infinite planar source, (b) set-up used to generate the slab voxel model and (c) voxel representation of the slab.

free path in the original slab. In other words, in the homogenized slab (which is $1/p$ times as thick as the original slab), the mean free path is $1/p$ times as long as the original one. Thus, the homogenized slab can be considered as a rescaling of the original slab.

The above result implies, for example, that the probability of n reactions per particle is the same in both cases. Then, there is a one-to-one correspondence between tracks in the homogenized and real slabs, the only difference being that in the voxel model, trajectories between reactions are dilated by $1/p$. As a consequence of this, the mean track length $\overline{L^*}$ in the homogenized slab is $1/p$ times the mean track length $\overline{L}$ in the real slab.

Now, the average fluence in a portion A of real slab (1 cm^2 of cross section and p cm thick) is proportional to the quotient between the mean track length in A and the volume of A (Carlsson 1985). Since tracks exiting A through the top face are compensated by tracks entering A through the bottom face and vice versa (and the same happens with the other faces), the average fluence can be computed as $N\overline{L}/(p\,\mathrm{cm}^3)$. Here, N is the number of incident particles traversing the 1 cm^2 cross section of A. On the other hand, the average fluence in a 1 cm^3 voxel of the homogenized slab is equal, for the same reasons, to $N\overline{L^*}/(1\,\mathrm{cm}^3) = N\overline{L}/(p\,\mathrm{cm}^3)$. As a result, the average fluence in both volumes coincides. Therefore, in this case, the average fluence in the portion A of real slab can be well estimated as the average fluence in the 1 cm^3 homogeneous cell. In the appendix to this paper, the average fluences in the real and homogenized slabs are explicitly computed for very low absorbing materials with small macroscopic scattering cross sections, obtaining the same result for both cases.

It is worth mentioning that slabs and sources do not need be infinite for these to be valid. If both the slab and the source are large enough, the portion of slab around the beam central axis behaves as in the idealistic situation. In fact, MCNP simulations using slabs with a

40×40 cm^2 cross section and planar disc sources of 5 cm radius give differences smaller than 3% between real and voxel geometries.

Now, consider an infinite parallelepiped phantom (i.e., a half-space geometry), placed with respect to the voxel grid in such a way that its p superficial centimetres lie in the first layer of the 1 cm^3 cells ($0 < p < 1$). The average fluence in this boundary portion of the phantom can also be described with great accuracy. The main difference between this problem and the previous one is that, in addition to the particle flux coming directly from the source, there is also a particle flux due to backscattering in the region contained in the following layers. However, this fluence can be considered as coming from a source in the back and acting on the thin slab of material contained in the first layer. In other words, the portion of phantom from the second layer on, acts on the first layer as another source. This source is the same for both the real and the homogenized cases. The way this source acts on the first layer coincides with the one described for the thin slab. Therefore, the average fluence in a portion of phantom contained in a cubic cell of the first layer can be well estimated as the average fluence in the homogenized cell of the voxel model. Again, this causes no significant error even if the phantom is not infinite but only large enough.

To summarize, in order to adjust the average fluence in the surface cells, the following strategy proves accurate for the parallelepiped phantom: the average fluence in the boundary portion of phantom contained in a cubic voxel is to be estimated by the average fluence in the whole cell of the voxel model.

To evaluate the fluence at every point of the modelled geometry, the average fluence in the surface voxel must be assigned to some point in space in order to carry out the interpolation/extrapolation process. Instead of assigning it to the centre of the voxel, the new strategy is *to assign it to the barycentre of the portion of the geometry contained in the voxel*. This gives as a result a very accurate estimation of average fluences in boundary areas and also improves the punctual estimation of the fluence.

In most clinical applications, the patient's anatomy is positioned in such a way that, around the beam central axis, the surface is approximately flat and the central axis is perpendicular to the local region. Therefore, the conclusions of the present analysis also hold for these boundary areas. For extreme cases such as the parallelepiped phantom in the angular position, the new strategy can be used to reassign the punctual fluence in the cases in which the centre of the voxel lies outside the phantom's edge (i.e., cases in which the voxel model assigns the average fluence in the cell to a point in the air).

To show the performance of this new strategy, it is tested in the parallelepiped phantom for the parallel position and also for the extreme case represented by the angular position.

2.4.2. Material percentage rounding. In all this reasoning, the effect of material percentage rounding was intentionally neglected. By the material assignment procedure described in section 2.1, the infinite p cm thick slab ($0 < p < 1$) leads to a homogenized mixture in which the proportion of slab material M is rounded to a multiple of 0.2. Clearly, the effect of rounding is greater when p is an odd multiple of 0.1. In these cases, the algorithm rounds down 0.1 the proportion of slab material (and rounds up the proportion of air). Note that from all odd multiples of 0.1, the one in which rounding has a more drastic effect is the case $p = 0.1$, since after rounding, the mixed material is only air. To quantify this in an example, assume that p is an odd multiple of 0.1, the particle source is planar and monodirectional, and that incident particles hit the slab surface perpendicularly and have at most one scattering reaction inside the slab. From equation (A.3) in the appendix, the relative difference between the average fluences for p and $p - 0.1$ can be obtained. This relative error is a decreasing function of p for $0.1 \leqslant p \leqslant 1$.

In consequence, to estimate the error caused by rounding, it is enough to deal with the case $p = 0.1$. If the average fluence in the slab is calculated as the average fluence in the homogenized cell, the result per particle entering the cell is 1 cm^{-2}, since in air it can be assumed that there are no scattering reactions. On the other hand, for any reasonable neutron energy and slab material, the mean free path is significantly greater than 0.1 cm. If the particles under consideration are photons, the mean free path is even greater. Then, particles can be assumed to undergo at most one scattering interaction in the slab. This situation is analogous to the one considered in the appendix, and the average fluence per particle entering the cell can then be computed as

$$\frac{\overline{\Phi}}{N} = \frac{1}{\boldsymbol{p}}\left(2\boldsymbol{p} - \frac{1}{\Sigma^M} + \frac{\mathrm{e}^{-p\Sigma}}{\Sigma^M}\right) = 2 + \frac{\mathrm{e}^{-\boldsymbol{p}\Sigma^M} - 1}{\boldsymbol{p}\Sigma^M} \tag{2}$$

(units are omitted for simplicity). Since $\boldsymbol{p} = 0.1$ cm, the second-order expansion of the exponential can be applied to obtain that this last expression is approximately $(1 + \boldsymbol{p}\Sigma^M/2)$ cm^{-2}. Therefore, the relative error due to rounding is

$$\frac{1 + \boldsymbol{p}\Sigma^M/2 - 1}{1 + \boldsymbol{p}\Sigma^M/2} = \frac{\boldsymbol{p}\Sigma^M}{2 + \boldsymbol{p}\Sigma^M} = \frac{0.1\Sigma^M}{2 + 0.1\Sigma^M}. \tag{3}$$

For values of Σ^M between 0 and 2 cm^{-1}, this represents in the worst case an error of 9%.

The derivation of equation (3) involves several assumptions. However, numerical MCNP simulations for an acrylic slab of variable thickness p cm ($0.1 < p < 1$), irradiated with two different neutron beams (a 5 keV monodirectional neutron beam of 5 cm radius and a real BNCT reactor source), show the decreasing behaviour of the relative error as a function of p, and maximum errors of 8% and 13% for the case $p = 0.1$, respectively. Note that these simulations are quite general considering ideal and real neutron sources and all possible reactions in the medium.

Finally, it is worth noting that with minor changes, this analysis can be carried out for any voxel cell size and any rounding percentage p. For example, equation (3) shows that the error due to rounding is approximately proportional to the rounded percentage. Therefore, this error can be reduced to a half by rounding material proportions to the closest 10% (instead of the closest 20%), and to a quarter by rounding to the closest 5%. As a counterpart, the number of mixture materials to handle would substantially increase: they would be 286 and 1771, respectively.

3. Results

3.1. Numerical test problems

Figures 2–5 summarize the results of the performance analysis for the parallelepiped phantom in parallel and angular positions. Statistical uncertainties in the simulation data amount to less than 1% and became imperceptible in all figures. The numerical reference—denoted as reference 1—corresponds to the 'punctual' thermal neutron fluence estimation along the beam axis derived from MCNP4c. For clarity, thermal neutron fluence profiles for only 5 of the 10 grid computed positions are depicted in figures 2 and 4.

As can be seen from figure 2, the thermal neutron fluence estimation is almost the same for all grid positions but it stands out that the best results are achieved when the voxel grid is adjusted to match up the phantom's entrance face (position 0). Note that for this position the homogenization process does not involve an expansion of the phantom's volume since the surface boundary voxels do not contain air.

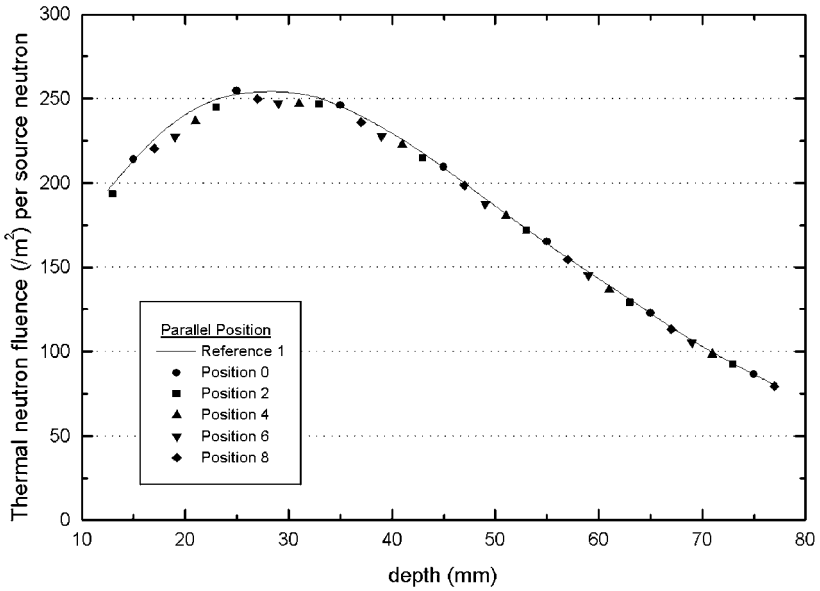

Figure 2. Comparison of the thermal neutron fluence profiles along the beam axis for the parallelepiped phantom in the parallel position. Reference 1 corresponds to the MCNP punctual reference data. Positions 0, 2, 4, 6 and 8 are the different locations of the voxel grid with respect to the phantom's entrance face.

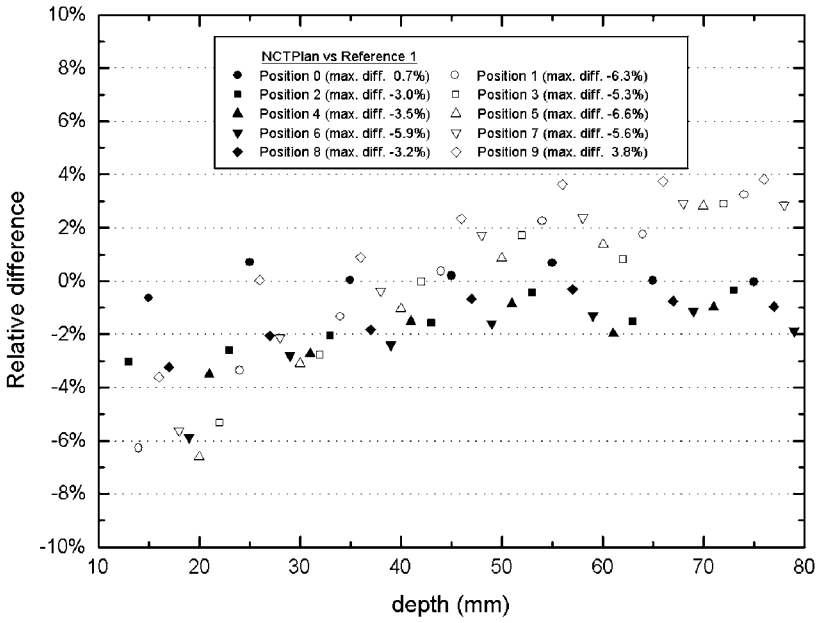

Figure 3. Percentage relative differences in thermal neutron fluences between the voxel model of the phantom in the parallel position (NCTPlan) and its corresponding punctual reference data (reference 1).

Figure 3 shows the percentage relative differences between the voxel method (NCTPlan) and reference data (reference 1), for the 10 computed positions. In the range of depths

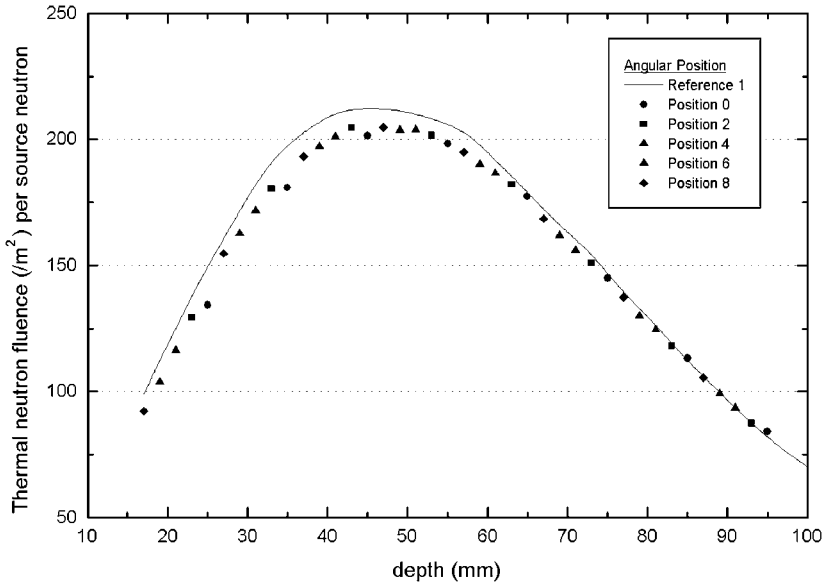

Figure 4. Comparison of the thermal neutron fluence profiles along the beam axis for the parallelepiped phantom in the angular position. Reference 1 corresponds to the MCNP punctual reference data. Positions 0, 2, 4, 6 and 8 are the different locations of the voxel grid with respect to the phantom's entrance edge.

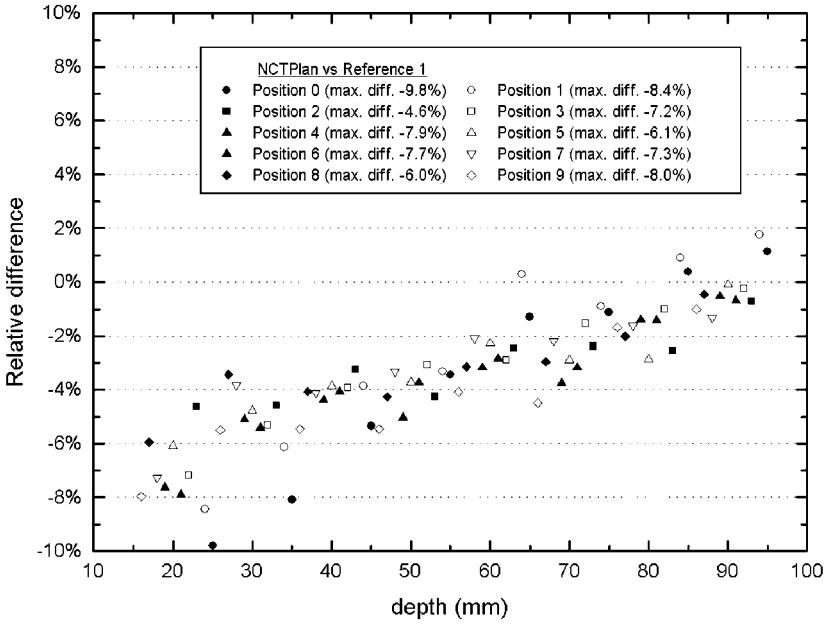

Figure 5. Percentage relative differences in thermal neutron fluences between the voxel model of the phantom in the angular position (NCTPlan) and its corresponding punctual reference data (reference 1).

considered in this analysis, position 5 provides the greatest maximum relative difference. This value agrees with the maximum difference between MacNCTPlan simulation and

MCNP reference data reported by Wojnecki and Green (2002), for the same simulation test.

Figure 4 shows the thermal neutron fluence profiles along the beam axis for the parallelepiped phantom in the angular position. Similarly to the parallel position, the fluence estimation is approximately the same for all grid positions but in this case, there seems not to be a preferred configuration. As shown in figure 5, the maximum relative difference between NCTPlan estimations and the reference data amounts to -9.8%, considering all grid computed positions. This value, which represents the worst case in the analysis, is less than half the maximum value reported by Wojnecki and Green (2002) for the MacNCTPlan algorithm (namely, -21.1%). Moreover, the large deviation observed at shallow depth (up to 60 mm) between the MCNP reference data and the results of the MacNCTPlan algorithm is not present in the case of NCTPlan simulations. Therefore, this analysis shows that the main reason for the lack of accuracy in the case of the MacNCTPlan voxel model is a deficiency in the material assignment strategy. Although the downsizing of the 1 cm^3 voxel size would improve the accuracy of the MacNCTPlan algorithm, for any fixed size the new algorithm leads to better results. In addition, the above results show that even in an extreme limit case, such as the irradiation of a sharp angled corner, the proposed 1 cm based voxel model provides good results. In fact, the accuracy obtained in the worst analysed case with this new algorithm is as good as that obtained with SERA's code (Nigg *et al* 1999) for the same simulation test (Wojnecki and Green 2002). While the maximum relative difference in the angular position amounts to -9.8% for the NCTPlan voxel model, a -10.6% maximum difference was reported for the SERA system.

Finally, all comparisons between NCTPlan and reference data are based on the referred 'punctual' thermal neutron fluence estimation. This imposes a greater challenge to the accuracy of the NCTPlan voxel model compared to the reference data tallied in 1 cm^3 volume in Wojnecki's work. The punctual estimation uses a very small tally volume of $\sim$3.1 mm^3 and therefore, this track length estimate will be close to the real thermal fluence at a point. On the other hand, the voxel model computes the thermal fluence in a 1 cm^3 volume. Since this track length estimate involves an average in a much larger volume around the axis containing maxima, the resulting thermal fluence will likely be lower than the punctual estimation (independently of the homogenization effects). Therefore, if a 1 cm^3 tally volume is used to compute reference values, a better agreement between simulations and reference data is obtained. The impact of the tally volume is discussed in detail later.

3.2. Dosimetry comparisons against experimental data

Figures 6(a)–(c) show the results of the comparative study based on the physical dosimetry of the RA-6 hyperthermal neutron beam measured in a cylindrical phantom (Blaumann *et al* 2004). Statistical uncertainties for numerical values are less than 1%. Figure 6(a) illustrates the thermal neutron flux profiles along the central beam axis. NCTPlan data agree most accurately with measurements, the absolute deviation of the experimental mean values being 7% on average, and the measurement uncertainties $\pm 8\%$. Figures 6(b)–(c) correspond to fast neutron and total gamma dose rate profiles specified for ICRU 46 adult muscle tissue. Both components show excellent agreement with measurements, the absolute deviation of the experimental mean values being 4% and 1% on average, and measurement uncertainties $\pm 32\%$ and $\pm 1\%$ for fast and gamma components, respectively.

It is important to stress that the RA-6 beam model used in this comparison was normalized to measurements carried out in the international reference cubic water phantom (Blaumann *et al* 2004). No other normalization procedure was applied between MCNP results

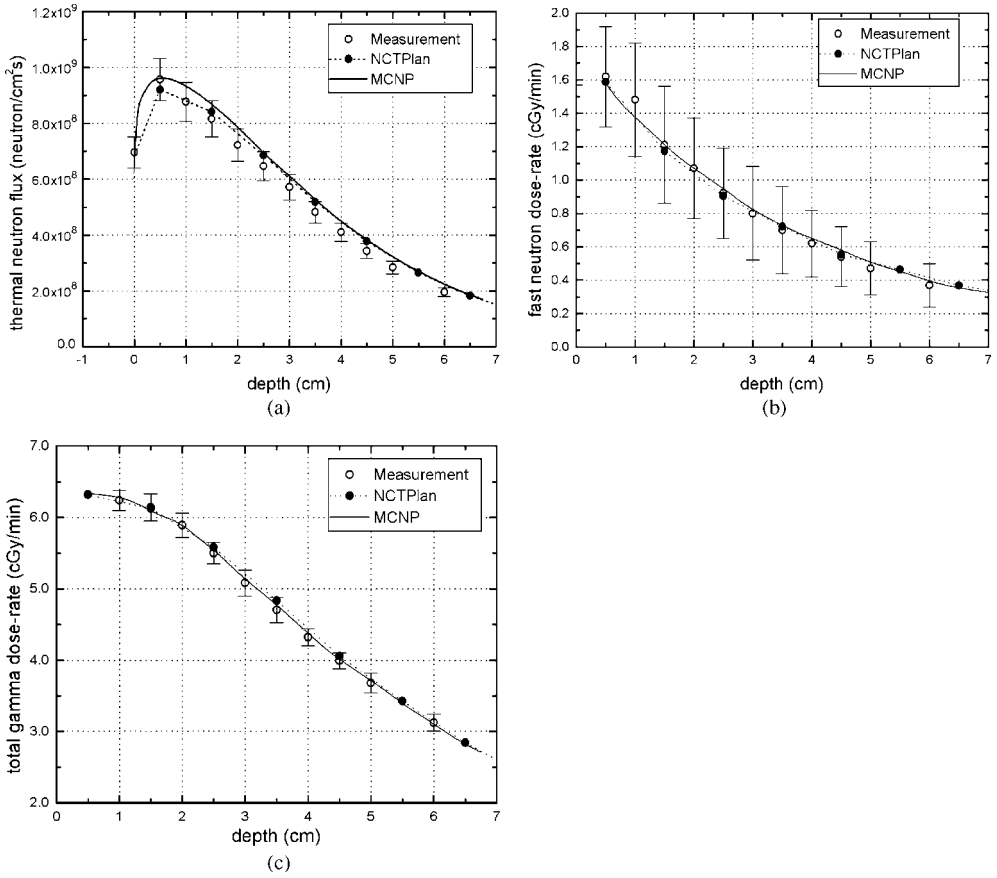

Figure 6. Comparison of measured and calculated dosimetries along the central axis of the RA-6 beam. (a) Thermal neutron flux versus depth in phantom. (b) and (c) Fast neutron and total gamma absorbed dose rate profiles specified for ICRU 46 adult muscle tissue versus depth in phantom.

and measurement in the cylindrical phantom. Then, the agreement in figures 6(a)–(c) indicates the goodness of the beam model to derive the dosimetry in other geometries. In addition, NCTPlan calculations also match up measurements without the need of any scaling factor, which indeed demonstrates the accuracy of the 1 cm based voxel model.

3.3. Reassignment strategy for surface voxels

Figure 7 illustrates the operation of the strategy proposed to improve the prediction of the punctual and average fluences within the first millimetres of the phantom surface. As can be observed, the thermal neutron fluences computed by the original voxel method for the parallel positions of the parallelepiped phantom (positions 0, 2, 4, 6 and 8) overestimate the reference values within the first 4 mm. The percentage relative differences between the original voxel model data and the punctual fluence (reference 1) range from 54% at 0 mm depth to 5% at 4 mm depth. However, if these differences are computed using the averaged fluence (reference 2), a maximum value of 18% is obtained. These results show that the deviation of the original voxel model from reference 1, though unavoidable, is not only due to the homogenization in surface cells but also to the averaging in a 1 cm^3 tally volume and the assignment of the average values to the centre of the cells. As shown in figure 7, when the new strategy is

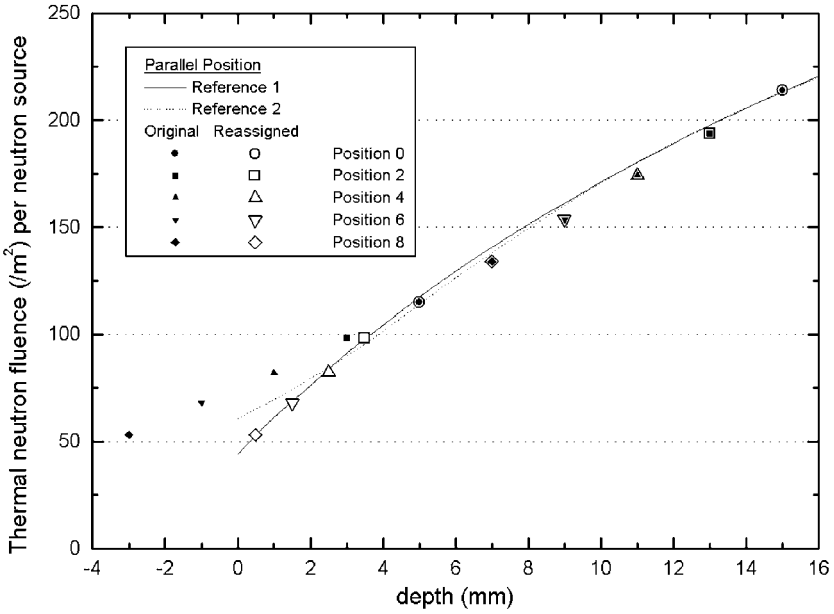

Figure 7. Comparison of the original and reassigned thermal neutron fluences in the first millimetres of the phantom surface. References 1 and 2 correspond to MCNP punctual and averaged reference data, respectively.

applied to compute fluence values at shallow depths, the agreement between reference 1 and the reassigned data is excellent. Percentage relative differences between these latter are 2% on average for positions 0, 2, 4, 6 and 8, and 12% on average for the remaining five positions. Note that for the odd grid positions, the differences between real and rounded material percentages in surface cells are maximum. If material percentages were not rounded for these cases, the resulting average deviation would be as low as for the even positions. It is important to remark that the largest deviations (54% and 18%) for the original assignment are forced by positioning the phantom with respect to the grid in a most disadvantageous way. In other words, even if the rules to position the phantom are not followed, accuracy is obtained with the proposed reassignment.

For the parallelepiped phantom in the angular position, the new strategy is used to reassign the punctual fluence in cases in which the geometric centre of the surface voxel lies outside the phantom's edge. For these cases, the percentage relative differences between the original voxel model data and the punctual fluence range from 140% to 56%. Again, the voxel method overestimates reference values. The same holds when the 1 cm^3 averaged fluence is used as the reference, but the maximum deviation is 32% in this case. Applying the strategy to reassign fluence values at shallow depths, the absolute value of the percentage relative differences decrease to 14% on average, with a maximum value of 23% at the surface of the phantom. Again, the largest deviations are intentionally obtained by positioning the phantom against the rules described above.

4. Discussion

In standard treatment planning systems for conventional radiotherapy, the time spent in dosimetry calculations is around 5 min. On the other hand, for a typical BNCT treatment plan, 50 million particle histories are usually tracked. This derives statistical uncertainties of 0.1%

and 2.5% for high- and low-dose regions, respectively. The process of photon and coupled neutron–photon fields takes approximately 2 h on a 2.4 GHz Pentium IV processor with 512 MB RAM. This execution time is achieved using a modified version of MCNP4B, and it can be reduced if calculations are processed on a cluster of computers (Goorley *et al* 2001a). Since the factor of speed-up is roughly the same as the number of computers used, a runtime similar to that involved in conventional radiotherapy could be attained. In attempting to improve the accuracy of the voxel model, two lines of action naturally arise: to reduce the 20% step for rounding material percentages and to decrease the voxel size.

A reduction in the rounding percentages increases the number of material mixtures to be considered in calculations. If the percentage step is set to 10%, the resulting number of materials is 286. The impact of this change in the computing time is not important, but the amount of memory utilized by the Monte Carlo code considerably increases. However, this should not be a problem for a reasonable modern computer and, as mentioned above, this change could reduce relative errors to a half in some surface areas. A percentage step of 5% would produce 1771 different material mixtures, which is impractical from the point of view of computation time and memory usage.

In Goorley *et al* (2002), the effect of decreasing the voxel size was studied. It was shown that MCNP execution times and required memory significantly increase if voxel size is reduced. Also, the improvements in dosimetry results are small and do not justify this cost. In Kumada *et al* (2004), the authors remarked that a reduction in the voxel size could lead to better results in the surface, but they reported that calculations performed with a voxel side of 0.5 cm would take approximately 10 times as long as with the 1 cm^3 voxel. Moreover, considerable improvements can be obtained with minimum computational cost with the reassignment strategy presented in this work. Another important point to consider for the voxel size selection, and thus the tally volume, is related to the size of the sensitive volume of ionization chambers employed in experimental measurements. The output current represents a spatial averaging of neutron–photon interactions occurring in a typical volume of the order of centimetres. Therefore, any reasonable comparison between experiment and calculation should involve tally volumes of this order of magnitude.

Another procedure to improve the accuracy at the surface follows from the results presented throughout this work. It is a simple rule that does not affect the execution time and memory usage. The anatomy images should be positioned with respect to the voxel grid in such a way that cells at the beam entrance are filled with a mixture with a minimum proportion of air. NCTPlan allows the user to examine the voxelized model, indicating the material mixture produced for each cell in it.

5. Conclusions

The performances of the 1 cm based voxel reconstruction methods used in the MacNCTPlan and NCTPlan treatment planning systems for BNCT were compared and analysed in detail. As a result, with the improved algorithms implemented by NCTPlan, the 1 cm resolution of the voxel method proves accurate enough for all presented tests, excluding very shallow depths in which, to achieve accuracy, the anatomy images need be positioned in a suitable way. Therefore, the MacNCTPlan material assignment algorithm is mainly responsible for the neutron thermal fluence deviations reported by Wojnecki and Green (2002). It should be noted that the NCTPlan voxel model was tested using simple and clinical-like geometries, using ideal and real BNCT neutron sources (epithermal and *hyperthermal* beams), and considering both numerical and experimental reference data. These latter involved the neutron flux and also the dose-rate components.

In addition, an investigation of the impact of the voxel grid position with respect to patient images led to guidelines to get the best performance of the current NCTPlan voxel model in surface boundary areas. The voxel model of a patient's anatomy should be built in order to minimize the proportion of air in surface cells around the beam entrance point.

In all BNCT treatments carried out at present, the skin is considered one of the organs at risk. Moreover, in the case of cutaneous melanoma in extremities, skin is essentially the organ that limits the delivered dose to the patient. Since surface boundary areas are those where homogenization can have a more distorting effect, the performance of the voxel model in these regions was analysed with special emphasis in this work.

A theoretical analysis was carried out to assess the distortion caused by homogenization and also to estimate the errors due to the materials percentage rounding process. Based on this analysis, a new strategy for the treatment of surface cells was proposed without any detriment to MCNP execution times. The performance of the new strategy was tested in two irradiation problems. For the parallelepiped phantom in parallel position, the large thermal neutron fluence deviation present at shallow depths (from 54% at 0 mm depth to 6% at 4 mm depth) was reduced to 2% on average. Reassigning fluence values in the case of the phantom in the angular position produced the maximum deviation in the thermal fluence to decrease from 140% to 23% at the surface of the phantom. Note that even if the rules to position the phantom images are not followed, as in the cases just presented, the reassignment provides very accurate estimates.

The mentioned results represent a substantial improvement to the performance of the voxel model in surface areas. Since the NCTPlan TPS is currently used in several BNCT projects, and in particular in the Argentine protocol for cutaneous melanomas in extremities, the new strategy will soon be implemented in the newer version of the NCTPlan code.

Acknowledgments

This work was supported by the Comisión Nacional de Energía Atómica (Argentina) and the International Atomic Energy Agency (under grant no ARG-00022P). The authors would also like to thank Herman Blaumann, Osvaldo Calzetta, Stead Kiger and Juan Longhino for their contributions and valuable comments.

Appendix

In this appendix, the average fluence in a 1 cm^2 cross section portion of an infinite slab is computed.

Consider an infinite p cm thick slab ($0 < p < 1$) of a low absorbing material M and macroscopic total cross section Σ^M, perpendicularly irradiated with a monodirectional neutron beam represented by an infinite planar source. If the particles' mean free path $1/\Sigma^M$ is sufficiently larger than p cm, they can be supposed to undergo at most one reaction inside the slab. Note that this condition is readily verified by photons for reasonable values of p and M. Besides, since M is a low absorbing material, only scattering reactions need be considered. For simplicity, we treat all particles as neutrons, but the analysis remains valid for photons.

As shown in section 2.4.1, the average neutron fluence in a portion A of this slab (A has 1 cm^2 of cross section and is p cm thick) can be estimated as

$$\overline{\Phi} = \frac{N\overline{L}}{p \text{ cm}^3}, \tag{A.1}$$

where N is the number of incident particles traversing the frontal 1 cm^2 cross section of A, and $\overline{L}$ is the mean track length of particles in the slab. This mean track length has then to be computed.

To simplify the notation in some formulae, let $\boldsymbol{p} = p$ cm be the slab thickness. The probability that a neutron does not suffer its first collision in the slab is $\mathrm{e}^{-p\Sigma^M}$. For these neutrons, the track length is exactly $\boldsymbol{p}$. On the other hand, a neutron has a collision inside the slab at r cm from the surface ($0 < r < p$) with a probability density of $\Sigma^M \mathrm{e}^{-r\Sigma^M}$ (here, $\boldsymbol{r} = r$ cm). For such a particle, the track length is $\boldsymbol{r} + (\boldsymbol{p} - \boldsymbol{r})/\cos(\theta)$, where θ is the angle between the beam direction and the neutron direction after the collision. Angles θ between 0 and $\pi/2$ occur with a probability density of $2\sin(\theta)\cos(\theta)$. Consequently, the mean track length of a particle can be computed as

$$\begin{aligned}
\overline{L} &= \int_0^p \int_0^{\pi/2} \left(\boldsymbol{r} + \frac{\boldsymbol{p}-\boldsymbol{r}}{\cos(\theta)}\right) 2\sin(\theta)\cos(\theta)\Sigma^M \mathrm{e}^{-\boldsymbol{r}\Sigma^M}\,\mathrm{d}\theta\,\mathrm{d}\boldsymbol{r} + \boldsymbol{p}\,\mathrm{e}^{-p\Sigma^M} \\
&= \int_0^p r\Sigma^M \mathrm{e}^{-\boldsymbol{r}\Sigma^M}\,\mathrm{d}r \int_0^{\pi/2} 2\sin(\theta)\cos(\theta)\,\mathrm{d}\theta \\
&\quad + \int_0^p (\boldsymbol{p}-\boldsymbol{r})\Sigma^M \mathrm{e}^{-\boldsymbol{r}\Sigma^M}\,\mathrm{d}\boldsymbol{r} \int_0^{\pi/2} 2\sin(\theta)\,\mathrm{d}\theta + \boldsymbol{p}\,\mathrm{e}^{-p\Sigma^M} \\
&= -\frac{\boldsymbol{p}\Sigma^M \mathrm{e}^{-p\Sigma^M} + \mathrm{e}^{-p\Sigma^M} - 1}{\Sigma^M} + 2\frac{\mathrm{e}^{-p\Sigma^M} + \boldsymbol{p}\Sigma^M - 1}{\Sigma^M} + \boldsymbol{p}\,\mathrm{e}^{-p\Sigma^M} \\
&= 2\boldsymbol{p} - \frac{1}{\Sigma^M} + \frac{\mathrm{e}^{-p\Sigma^M}}{\Sigma^M}. \qquad \text{(A.2)}
\end{aligned}$$

Substituting expression (A.2) into equation (A.1), the average fluence in the portion of slab A is therefore

$$\overline{\Phi} = \frac{N}{p\ \mathrm{cm}^3}\left(2\boldsymbol{p} - \frac{1}{\Sigma^M} + \frac{\mathrm{e}^{-p\Sigma^M}}{\Sigma^M}\right) = \frac{N}{\mathrm{cm}^2}\left(2 - \frac{1}{\boldsymbol{p}\Sigma^M} + \frac{\mathrm{e}^{-p\Sigma^M}}{\boldsymbol{p}\Sigma^M}\right). \qquad \text{(A.3)}$$

Now, if the mean track length is computed in a 1 cm^3 cell of the voxel model of the infinite slab, a material mixture M^* consisting of a proportion p of M and $(1-p)$ of air has to be considered. As observed in section 2.4.1, this can be seen as a new slab 1 cm thick with a macroscopic cross section of approximately $p\Sigma^M$. Therefore, proceeding as before, the mean track length is 2 cm $- \frac{1}{p\Sigma^M} + \frac{\mathrm{e}^{-p\Sigma^M}}{p\Sigma^M}$, and consequently, the average fluence in a 1 cm^3 cell is $\frac{N}{\mathrm{cm}^3}\left(2\ \mathrm{cm} - \frac{1}{p\Sigma^M} + \frac{\mathrm{e}^{-p\Sigma^M}}{p\Sigma^M}\right)$, which coincides with the average fluence obtained for the original slab.

References

Attix F H 1986 *Introduction to Radiological Physics and Radiation Dosimetry* (New York: Wiley)

Blaumann H R, González S J, Longhino J, Santa Cruz G A, Calzetta Larrieu O A, Bonomi M R and Roth B M C 2004 Boron neutron capture therapy of skin melanomas at the RA-6 reactor: a procedural approach to beam set up and performance evaluation for upcoming clinical trials *Med. Phys.* **31** 70–80

Briesmeister J F 1997 *MCNP^{TM}—A General Monte Carlo N-Particle Transport Code 12625-M* (Los Alamos, CA: University of California)

Carlsson G A 1985 Theoretical basis for dosimetry *The Dosimetry of Ionizing Radiation* (London: Academic)

Cerullo N and Daquino G 2001 A treatment planning system based on real boron distribution and MCNP-4^a code: results and discussion *Frontiers in Neutron Capture Therapy* vol 1, ed M Hawthorne, K Shelly and R Wiersema (New York: Kluwer/Plenum) pp 225–30

Coderre J A and Morris G M 1999 The radiation biology of boron neutron capture therapy *Radiat. Res.* **151** 1–18

Duderstadt J J and Martin W R 1979 *Transport Theory* (New York: Wiley)

González S J *et al* 2004 First BNCT treatment of a skin melanoma in Argentina: dosimetric analysis and clinical outcome *Appl. Radiat. Isotopes* **61** 1101–5

González S J, Santa Cruz G A, Kiger W S III, Goorley J T, Palmer M R, Busse P M and Zamenhof R G 2002 NCTPlan, the new PC version of MacNCTPlan: improvements and verification of a BNCT treatment planning system *Proc. 10th Int. Congress on Neutron Capture Therapy* ed W Sauerwein, R Moss and A Wittig (Bologna: Monduzzi Editore, International Proceedings Division) pp 557–61

Goorley J T, Kiger W S III and Zamenhof R G 2002 Reference dosimetry calculations for neutron capture therapy with comparison of analytical and voxel models *Med. Phys.* **29** 145–56

Goorley J T, McKinney G, Adams K and Estes G 2001a MCNP enhancements, parallel computing and error analysis for BNCT *Frontiers in Neutron Capture Therapy* vol 1, ed M Hawthorne, K Shelly and R Wiersema (New York: Kluwer/Plenum) pp 599–604

Goorley T, Wheeler F, Capala J, Kiger W S III, Palmer M and Zamenhof R 2001b A comparison of two BNCT treatment planning programs: MacNCTPlan and BNCT_RTPE *Frontiers in Neutron Capture Therapy* vol 1, ed M Hawthorne, K Shelly and R Wiersema (New York: Kluwer/Plenum) pp 207–12

ICRU 1992 Photon, electron, proton and neutron interaction data for body tissues *International Commission on Radiation Units and Measurements Report* 46 (Bethesda, MD: ICRU)

ICRU 1999 Nuclear data for neutron and proton radiotherapy and for radiation protection *International Commission on Radiation Units and Measurements Report* 63 (Bethesda, MD: ICRU)

Ingersoll D T, Slater C O, Redmond E L and Zamenhof R G 1997 Comparison of TORT and MCNP dose calculations for BNCT treatment planning *Advances in Neutron Capture Therapy* vol I, ed B Larsson, J Crawford and R Weinreich (Amsterdam: Elsevier) pp 95–9

Kiger W S III, Zamenhof R G, Solares G R, Redmond E L II and Yam C S 1996 MacNCTPlan: an improved Macintosh-based treatment planning program for boron neutron capture therapy *Trans. Am. Nucl. Soc.* **75** 38

Kotiluoto P, Hiismäki P and Savolainen S 2001 Application of the new MultiTrans SP_3 radiation transport code in BNCT dose planning *Med. Phys.* **28** 1905–10

Kumada H, Yamamoto K, Matsumura A, Yamamoto T, Nakagawa Y, Nakai K and Kageji T 2004 Verification of the computational dosimetry system in JAERI (JCDS) for boron neutron capture therapy *Phys. Med. Biol.* **49** 3353–65

Locher G L 1936 Biological effects and therapeutic possibilities of neutrons *Am. J. Roentgenol.* **36** 1–13

Mackerle J 2003 Topology and shape optimization of structures using FEM and BEM: a bibliography (1999–2001) *Finite Elem. Anal. Des.* **39** 243–53

Moran J M, Nigg D W, Wheeler F J and Bauer W F 1992 Macroscopic geometric heterogeneity effects in radiation dose distribution analysis for boron neutron capture therapy *Med. Phys.* **19** 723–32

Moulton J D 1996 Nodal methods: analysis, performance and fast iterative solvers *PhD Thesis* University of British Columbia

Nigg D W, Wemple C A, Wessol D E, Wheeler F J, Algright C, Cohen M, Frandsen M, Harkin G and Rossmeier M 1999 SERA—an advanced treatment planning system for neutron therapy and BNCT *Trans. Am. Nucl. Soc.* **80** 66–8

Rogus R D, Harling O K and Yanch Y C 1994 Mixed field dosimetry of experimental neutron beams for boron neutron capture therapy at the MITR-II research reactor *Med. Phys.* **21** 1611–25

Smith K S 1986 Assembly homogenization techniques for light water reactor analysis *Prog. Nucl. Energy* **17** 303–35

van der Zee S C, Hogenbirk A and van der Marck S C 2002 Orange, a Monte Carlo dose engine for BNCT *Proc. 10th Int. Congress on Neutron Capture Therapy* ed W Sauerwein, R Moss and A Wittig (Bologna: Monduzzi Editore, International Proceedings Division) pp 569–72

Wazer D E, Zamenhof R G, Harling O K and Madoc-Jones H 1994 Boron neutron capture therapy *Radiation Oncology: Technology and Biology* ed P Mauch and J Loeffler (Philadelphia, PA: Saunders)

Wojnecki C and Green S 2002 A preliminary comparative study of two treatment planning systems developed for neutron capture therapy: MacNCTPlan and SERA *Med. Phys.* **29** 1710–5

Zamenhof R, Busse P, Harling O and Goorley J T 1999 Boron neutron capture therapy *The Modern Technology of Radiation Oncology: A Compendium for Medical Physicist and Radiation Oncologist* ed J Van Dyk (Madison, WI: Medical Physics Publishing)

Zamenhof R, Redmond E II, Solares G, Katz D, Riley K, Kiger S and Harling O 1996 Monte Carlo-based treatment planning for boron neutron capture therapy using custom designed models automatically generated from CT data *Int. J. Radiat. Oncol. Biol. Phys.* **35** 383–97